# 論文 / 著書情報
# Article / Book Information

| | |
|---|---|
| Title | Uncertainty reduction in power forecasting of virtual power plant: From day-ahead to balancing markets |
| Authors | Reza Nadimi, Mika Goto |
| Citation | Renewable Energy, Vol. 238, , |
| Pub. date | 2024, 11 |
| DOI | https://dx.doi.org/10.1016/j.renene.2024.121875 |

Renewable Energy 238 (2025) 121875

Contents lists available at ScienceDirect

Renewable Energy

journal homepage: www.elsevier.com/locate/renene

# Uncertainty reduction in power forecasting of virtual power plant: From day-ahead to balancing markets

Reza Nadimi *, Mika Goto

*Department of Innovation Science, School of Environment and Society, Institute of Science Tokyo, 3-3-6, Shibaura, Minato-ku, Tokyo, 108-0023, Japan*

ARTICLE INFO

*Keywords:*
Uncertainty in bidding
Virtual power plant
Electricity balancing market
And long short-term memory prediction model

ABSTRACT

Adjusting prediction data before bidding is a straightforward and cost-effective method to reduce uncertainty and imbalance between bidding data and real-time power supply. To avoid profit loss for virtual power plant, this study proposes an uncertainty optimization model that minimizes the remaining uncertainty after power generation forecasts. The proposed model specifically addresses different weather conditions—rainy, overcast, cloudy, partly cloudy, and sunny—by minimizing the distance between actual and forecasted VPP generation. The model is applied to adjust prediction data of a VPP with an average generation capacity of 1.5 GW in Tokyo, Japan. Bidding data for winter 2024 are predicted using three deep neural network-based methods. The results indicate a significant reduction in both uncertainty and energy storage capacity after using the uncertainty optimization model. Moreover, the findings show that the proposed uncertainty optimization model increases the profit growth rate for prediction methods characterized by high uncertainty.

Nomenclature

**Majority of variables' format:** $A_C^{B,D}$

**A** refers to Demand, Generation, Supply, Price, Surplus, State of charge (SOC), Cost, or Binary/Slack variables,

**B** specifies the source of power supply (technology), demand sources, market types, or negative/positive slack variable

**C** indicates the settlement period, or the minimum or maximum capacity for a technology, and

**D** represents additional information such as estimated or actual power supply,

For example, $S_t^{grid,E}$: represents estimated grid supply power at settlement period $t$.

| **Input Variables** | **Description** | **Unit** |
|---|---|---|
| $P_t^{DA}$ | Day-ahead power price at period $t$ | $/kW |
| $P_t^{ID}$ | Intra-day power price at period $t$ | $/kW |
| $P_t^{Bal}$ | Balance cost at period $t$ | $/kW |
| $R_t^{su}$ | Random number generated from standard uniform distribution at period $t$ | – |
| $R_t^h$ | Historical percentage of contract's number at period $t$ (per maximum daily contract) | – |
| $S_t^{VPP,E}$ | Estimated VPP power supply at period $t$ | kW |
| $S_t^{VPP,Bid}$ | VPP power supply based on bid data for DA (ID) market at period $t$ | kW |
| $S_t^{VPP,A}$ | Actual VPP power supply at period $t$ | kW |
| $\lambda_{1,2,3,4,t}$, $\alpha_{1,2,3,4,5,t}$ | Trading transition probability at period $t$ | % |
| **Intermediate Variables** | **Description** | **Unit** |
| $SOC_t^{Bat}$ | Battery state of charge at period $t$ | kW |

(*continued on next column*)

(*continued*)

| **Decision variable** | **Description** | **Unit** |
|---|---|---|
| Continuous | | |
| $S_t^{Bat,disch}$ | Discharging power from battery at period $t$ | kW |
| $S_t^{Bat,ch}$ | Charging power into battery at period $t$ | kW |
| $S_t^{grid,E}$ | Estimated grid power supply at period $t$ | kW |
| $S_t^{grid,E,ID}$ | Estimated grid power supply in the ID market at period $t$ | kW |
| $S_t^{grid,E,Bal}$ | Estimated grid power supply in the Balance market at period $t$ | kW |
| $S_t^{grid,A,ID}$ | Actual grid power supply in the ID market at period $t$ | kW |
| $S_t^{grid,A,Bal}$ | Actual grid power supply in the Balance market at period $t$ | kW |
| $Su_t^{VPP,ID}$ | VPP surplus power in the ID market at period $t$ | kW |
| $Su_t^{VPP,Bal}$ | VPP surplus power in the Balance market at period $t$ | kW |
| $\theta_{t,j}$ | prediction uncertainty for $j$th type of days at period $t$ | – |
| Binary | | |
| $B^{DA}$ | Binary variable for day-ahead market | |
| $B_t^{Bat,ch}$ | Binary variable for battery charging at period $t$ | {0,1} |
| $B_t^{Bat,disch}$ | Binary variable for battery discharging at period $t$ | {0,1} |
| **Slack variable** | **Description** | **Unit** |
| $S_t^{Negative}$ | Negative slack variable at period $t$ | kW |

(*continued on next page*)

* Corresponding author.
*E-mail address:* rn.nadimi@gmail.com (R. Nadimi).

https://doi.org/10.1016/j.renene.2024.121875
Received 31 July 2024; Received in revised form 7 October 2024; Accepted 10 November 2024
Available online 15 November 2024

(*continued*)

| | | |
|---|---|---|
| $Sl_t^{Positive}$ | Positive slack variable at period $t$ | kW |
| **Model Parameters** | **Description** | **Unit** |
| $S_{max}^{Bat.disch}$ | Maximum discharging power from battery at period $t$ | kW |
| $C^{VPP}$ | Operation cost of VPP | $/kW |
| $SOC^{max}$ | Maximum SOC of battery (80 % of battery capacity) | kWh |
| $SOC^{min}$ | Minimum SOC of battery (20 % of battery capacity) | kWh |
| $\eta_{ch}^{Bat}$ | Battery charging efficiency | % |
| $\eta_{disch}^{Bat}$ | Battery discharging efficiency | % |
| $\Phi_{DA}$ | Minimum power requirement (MPR) for DA market | kW |
| $\Phi_{ID}$ | MPR for ID market | kW |
| **Other symbols** | **Description** | |
| JEPX | Japan Electric Power Exchange | – |
| $M_1$ | Big number or Big-M (here $M_1$ = initial battery capacity) | – |

## 1. Introduction

The system operator continually balances power generation and consumption due to the existence of uncertainty in the grid network, while the imbalance is inevitable. Synchronous power generators use inertia to balance the supply and demand via maintaining a stable[1] frequency. However, the high penetration of inverter-based generators[2] —such as wind power, solar power, and batteries— reduces the overall inertia of the generation system, thereby increasing system imbalance [1].

The balancing market manages system imbalance via independent system operators, balancing service providers, and balance-responsible parties [2]. These parties utilize demand response [3], reserve capacity plans [4], and market contributions [5,6] to maintain system balance. As a power supplier, virtual power plants (VPPs) take different actions to mitigate unplanned fluctuations in power supply. The actions taken by VPPs to reduce imbalance consist of rescheduling generation technologies, utilizing energy storage, and using accurate prediction methods [7,8].

VPP power supply is predicted through stochastic[3] [9,10] and artificial neural network approaches [11,12]. Long Short-Term Memory (LSTM) and Bidirectional LSTM (BiLSTM) are two prominent deep learning methods that have demonstrated superiority over stochastic methods in multi-step ahead predictions [11]. These methods effectively predict solar and wind power generation for several hours ahead. The VPP system requires highly accurate methods to predict its power supply for longer than 24 h. Appendix A provides details information of the Decision Support System BiLSTM model (DSS-BiLSTM), which forecasts the VPP power generation 38 h ahead, outperforming both LSTM and BiLSTM methods. This study utilizes the three mentioned methods to forecast the power generation of a VPP with an average generation capacity of 1.5 GW in Tokyo, Japan.

Assuming fixed power demand, the VPP generation imbalance indicates the gap between actual and planned (bidding data) power generation. This gap represents the uncertainty faced by the VPP in fulfilling its commitments in short-term power markets, such as the Day-Ahead (DA) and Intra-Day (ID) markets. Although prediction models are designed to minimize this gap, a degree of uncertainty remains, particularly in DA prediction models that extend over long timeframes. VPP owners can measure this remaining uncertainty via comparing historical generation data with prediction data. This residual uncertainty can lead to a loss of planned profit within the ID and balancing markets. Moreover, t uncertainty magnifies the ID trading transactions, while may impose additional imbalance burdens on the balancing market. ID trading occurs when the VPP system updates its prediction data a few hours before the dispatch time, and the prediction data may change again until the gate closure.

*Research Contribution*: The primary contribution of this study is the proposal of an Uncertainty Optimization (UO) model aimed at mitigating the uncertainty that persists following the initial prediction model. By addressing a portion of this residual uncertainty, the UO model enhances profitability for VPPs, reduces the magnitude of VPP imbalances, and decreases the estimated capacity required for energy storage. In contrast to numerous studies that focus solely on one or two short-term markets [35], this research adopts a comprehensive approach by concurrently considering the DA, ID, and balancing markets.

The paper's structure is as follows: Section 2 reviews VPP uncertainty reduction research in electricity market. Section 3 describes and formulates the uncertainty reduction problem along with the proposed UO model for solving the problem. Section 4 represents the results of the proposed model. Section 5 discusses the findings of the current research and unrolls the main results. Section 6 summarizes the main results and implication of the proposed model.

## 2. Literature review and research objective

The major sources of imbalance volume in the power market are renewable power and demand load, with VPP systems relying primarily on renewable energy resources. Recent studies on VPPs have largely engaged with allocating resources, optimizing operational strategies, and mitigating uncertainty [13]. Intermittent renewable energy resources, demand load fluctuations, and power market factors are three main sources of uncertainty in the VPP system [14].

Uncertainty associated with renewables can be reduced via accurate forecasting models, multiple renewable generation technologies, and out-of-market actions. Various methods have been applied to predict renewable power generation and demand load based on physical, statistical, and artificial neural network methods. These approaches have been used either as a single or hybrid method to narrow down the gap between the forecasted values and actual power generation (uncertainty). Key sources of demand uncertainty include demand load predictions, seasonal heating and cooling load predictions, and out-of-market actions. Additionally, market uncertainty can be minimized by accurate market price forecasting and by considering market design parameters, such as gate closure and settlement procedures.

*Motivation*: As given in Table 1, accurate forecasting is one of the key ways to mitigate uncertainty because inaccurate prediction puts a burden of imbalance cost on VPP owners. According to Table 1, the LSTM and BiLSTM models are frequently used in forecasting because of their superiority over the stochastic methods [15–17]. The advantages of these models include:

- Enhanced accuracy in forecasts, which contributes to uncertainty reduction,
- Robust memory capabilities that facilitate the retention of relevant information over extended sequences,
- Bidirectional processing that allows for the consideration of both past and future data, and
- Reliable predictions even in the presence of noise and non-linearity.

Despite the improvements these models provide in narrowing the gap between actual and predicted data, some uncertainty remains unaddressed. A comparison of actual historical data with historical forecasting data unfolds the existence of uncertainty, particularly in less accurate prediction models. This problem widens the gap between

[1] Ability of the grid to respond to a contingency event.

[2] Geothermal, biomass, concentrating solar power, and hydropower belong to the synchronous generators.

[3] Such as autoregressive (AR), autoregressive integrated moving average (ARIMA), seasonal ARIMA (SARIMA), and SARIMA plus exogenous variables (SARIMAX).

**Table 1**
VPP uncertainty sources and their mitigation ways.

| Uncertainty sources | Uncertainty reduction by | Explanations and references |
|---|---|---|
| **Renewable energy** | -Prediction | ❖ Reducing solar power uncertainty via deep learning techniques, primarily LSTM and BiLSTM, as well as statistical prediction models [11,18,20],<br>❖ Utilizing deep learning methods such as LSTM and BiLSTM to effectively forecast wind power and lessen wind power uncertainty [15,21,22], |
| | -Multiple generation technologies | ❖ Integrating several renewable energy technologies (such as wind-solar, solar-hydro, or solar-wind-hydro) to reduce generation uncertainty [23,24],<br>❖ Utilizing energy storage along with renewable energy resources to balance the mismatch between generation and consumption [25,26]. |
| | -Out-of-market actions | ❖ Devoting part of power forecasting for internal balance [27]. |
| **Demand load** | -Load forecasting | ❖ Applying artificial neural network models to accurately forecast demand load and reduce uncertainty [19,28], |
| | -Seasonal load prediction | ❖ Identifying monthly variability in electricity usage, daily peak load scale, and daily peak load timing to predict, manage, and save residential electricity usage [29,30].<br>❖ Optimizing residential energy usage and building design parameters via forecasting of cooling and heating loads [31,32]. |
| | -Out-of-market actions | ❖ Intentionally augmenting the load forecasting value by the system operator to secure the electricity supply and avoid shortfalls in generation capacity [33]. |
| **Market factors** | -Market price | ❖ DA market price prediction: 1) Assessment of the potential revenue from the DA market in the presence of less-predictable renewable energy resources, energy storage costs, and power transmission costs, 2) Analyzing market price volatility with an increase in the penetration rate of renewable energy resources [34].<br>❖ ID market price prediction: Assessment of potential revenue from the ID market amid low liquidity, high price volatility, less-predictable renewable energy resources, costs of unplanned outages (short duration), ID price dynamics, and compensation of the DA market's imbalance [35,36].<br>❖ Balance market price prediction: Assessment of potential revenue from the balancing market in the presence of less-predictable renewable energy resources, costs of unplanned outages (very short duration), and adjustment costs of ID market predictions [37,38]. |
| | -Gate closure[a] | ❖ Shortening the gate closure to reduce demand and supply uncertainty, despite a slight increase in the system's operational costs [39].<br>❖ Shortening the gate closure to decline short-term price variation, despite its insignificant effect on the long-term [40]. |
| | -Settlement procedure | ❖ Introducing penalty costs (symmetric or asymmetric) based on single (or dual) prices to encourage (or discourage) market participants to forecast precisely (or engage in arbitrage) and shrink power volume imbalances in real-time due to the expansion of renewable energy resources [41], |

[a] Germany, Belgium and The Netherlands have set 15-min for their balancing gate closure time (BGCT), while France and Finland have set 60-min for their BGCT.

bidding data and real-time generation, potentially leading to profit loss for VPP due to balancing cost.

*Research objection*: The main objective of this study is to reduce uncertainty that persists following the initial prediction model. To address this challenge, this study proposes the uncertainty optimization model designed specifically to mitigate this residual uncertainty. The output of the UO model consists of coefficients used to adjust the initial prediction data based on varying weather conditions —namely, rainy, overcast, cloudy, partly cloudy, and sunny days. The UO model minimizes the distance between actual and predicted data for each of these weather conditions across 48 settlement periods to generate 48 corresponding coefficients. These coefficients will reduce the uncertainty remained after the initial forecasting mZodel.

## 3. Methodology

Fig. 1 illustrates the timeline of the DA and ID markets in the JEPX market. The settlement period in the JEPX market is 30 min, comprising 48 daily dispatch products, while the gate closure interval is 1 h before each dispatch time. As a supplier, the VPP system is allowed to submit its DA bids from 8:00 to 10:00 a.m. on the current day. In order to decrease the gap between the bidding data and dispatch power (real-time power), the VPP may rely on prediction results up until the last moment (before gate closure). The DA prediction is carried out at least 14 h before the first dispatch time, with a prediction length of at least 38 h (from 10:00 a.m. on the current day to 4:30 p.m. on the following day). The DA bidding data, which is submitted only once per day, is constructed based on the DA prediction data. In contrast, ID market predictions are carried out for each settlement period in a rolling horizon format.

Generally, the VPP owner can adjust specific DA bidding data up to 7 h before its corresponding dispatch time. This adjustment period can last for 6 h (12 times), because of the gate closure occurring 1 h before each dispatch product. Instead of 12 times, this study assesses the effect of DA bidding adjustment in the ID market for three times (see Fig. 1). The first bidding data is adjusted at 17:00, 22:00, and 23:00 corresponding to 7 h, 2 h, and 1 h before the first dispatch product (Dispatch {1}). After each prediction, the bidding data is adjusted, and shortage and surplus power are traded in the ID market.

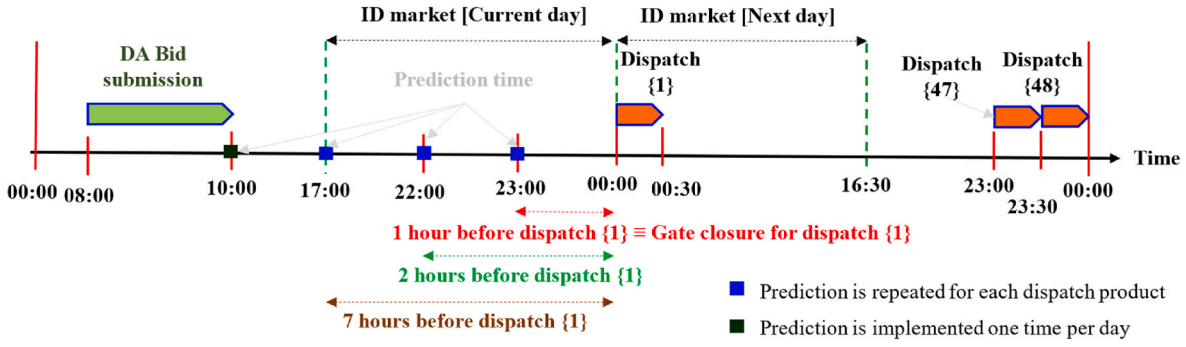


**Fig. 1.** Day-ahead and intraday markets time-line in JEPX.

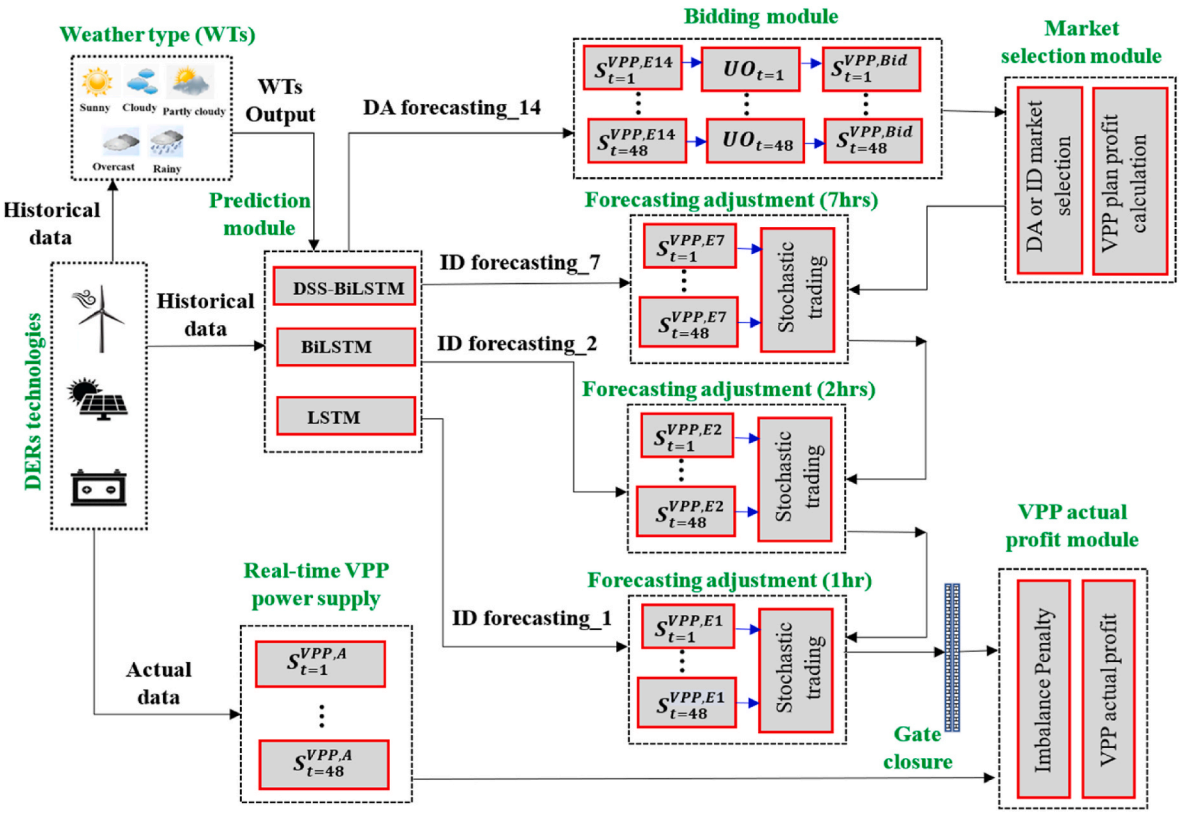


**Fig. 2.** Schematic framework of the proposed VPP profit calculation model (Note: DA forecasting_14 indicates that the VPP power supply is forecasted 14 h before the first dispatch and lasts for 38 h. ID forecasting_*h* indicates that the VPP power supply is forecasted *h* hours before each dispatch.).

As shown in Fig. 2, this study creates three sets of bidding data corresponding to the LSTM, Bi-LSTM, and DSS-BiLSTM prediction models. These models are applied to estimate DERs power generation (or VPP power supply, $S_t^{VPP,E}$) via historical DER data. It is noticeable that the UO model operates independently of the prediction model. However, to assess the effectiveness of the UO model in terms of the prediction model, this study investigates three prediction models with varying levels of accuracy. The role of the prediction model is to reduce uncertainty between bidding data and real-time power data. In contrast, the role of the UO model is to remove additional uncertainty present in the forecasting data that the prediction model cannot address.

The UO model conducts uncertainty optimization and calculates 48 coefficients corresponding to each settlement period. The coefficient values vary in terms of weather conditions: rainy, overcast, cloudy, partly cloudy, and sunny days. These five types of days are determined using historical DERs data via the K-Means clustering algorithm in the Weather Types (WTs) module. The bidding value, $S_t^{VPP,Bid}$, is calculated by multiplying $S_t^{VPP,E}$ by the corresponding coefficient. The market selection module utilizes the bidding data within an optimization model to specify whether the DA or ID market is more profitable for the VPP system. The stochastic plan provides probabilistic insights to balance VPP deviations in the ID market. According to this stochastic plan, the VPP owner may be unable to buy (or sell) its shortage (or surplus) power in the ID or balancing market. In the balancing market, transmission system operator takes actions to settle any deviation (shortage or surplus power) between planned and actual generation. The actual profit module calculates the actual VPP profit based on bidding data, adjustment data, and real-time data. The framework also includes other modules, which are explained below.

### 3.1. WTs module

The WTs module figures out whether a specific day is sunny, partly cloudy, cloudy, overcast, or rainy through maximum daily VPP power generation data and clustering method as follows:

**Step1)** Calculate the maximum daily VPP power generation:

$$y_i = \max\left(S_{t=1}^{VPP,A}, \ldots, S_{t=48}^{VPP,A}\right), i = 1, 2, \ldots, number\ of\ days \quad (1)$$

Weather variations ranges from the minimum $y_i$ (rainy day) to the maximum $y_i$ (sunny day).

**Step2)** Cluster the $y_i$ data into five weather types: The maximum daily power generation is clustered into five categories —rainy, overcast, cloudy, partly cloudy, and sunny—using the K-means clustering method [42], based on the variance ratio criterion [43]. The boundaries of these clusters are stored in the database, as shown in Fig.A.1 of Appendix A.

### 3.2. Bidding module

The bidding module calculates the bidding data with the lowest uncertainty in VPP power generation. This power generation uncertainty minimizes the distance between the predicted and actual historical data for each settlement period in terms of WTs. As shown in Fig. 3, the minimization problem figures out $\theta_{t,j}$, which indicates the extent to which the total prediction uncertainty can be reduced for the settlement period of $t$ and $j$th type of WTs. According to the historical data, the following least squared model is used to minimize the prediction uncertainty for the $j$th type of WTs:

$$min\sum_{j}\left(S_{t,j}^{VPP,A}-\theta_{t,j}S_{t,j}^{VPP,E}\right)^2 \quad s.t. \quad 0<\theta_{t,j}\le 1, t=\{1,2,\ldots,48\} \tag{2}$$

The bidding data is calculated as follow for the settlement period of $t$ and $j$th type of weather:

$$S_{t,j}^{VPP,Bid}=\theta_{t,j}S_{t,j}^{VPP,E} \tag{3}$$

where $S_{t,j}^{VPP,E}=0$ *if* $S_{t,j}^{VPP,E}\le\Phi_{DA}$ *or* $S_{t,j}^{VPP,E}\le\Phi_{ID}$. It is noticeable that the subscript $j$ is just for the separation of the day type. Thus, once the weather type is determined and data is filtered based on day type, the subscript $j$ is dropped out from the equations above.

### 3.3. Market selection module

The market selection module runs a mixed-integer optimization problem to choose between the DA or ID market based on the expected profit of the VPP system during the planning phase. Equation (4) represents the expected objective function of this optimization problem.

$$Max\sum_{t=1}^{48}\left[S_t^{VPP,Bid}\left(B^{DA}\left[P_t^{DA}(1-\varnothing)-S_t^{grid,E,ID}P_t^{ID}\lambda_{1,t}-S_t^{grid,E,Bal}P_t^{Bal}\lambda_{2,t}\right]+\left(1-B^{DA}\right)\left[P_t^{ID}-S_t^{grid,E,ID}P_t^{ID}\lambda_{3,t}-S_t^{grid,E,Bal}P_t^{Bal}\lambda_{4,t}\right]\right)-S_t^{VPP,E}C^{VPP}\right] \tag{4}$$

where ∅ represents the reserve capacity percentage, which is considered only for the DA market. The reserve capacity indicates the available capacity to deal any contingency, with the associated cost borne solely consumers in Japan. However, the reserve capacity cost is proportionally shared between suppliers and consumers [44]. The area served by TEPCO must maintain at least 5 % reserve capacity to avoid the blackout risk [45]. The amount of $S_t^{VPP,Bid}$ is adjusted for the DA and ID markets based on Equations (5) and (6), respectively, to meet the minimum market requirements.

$$S_t^{VPP,Bid}=\begin{cases}S_t^{VPP,E} & if\ S_t^{VPP,E}\ge\Phi_{DA}\\ 0 & o.w.\end{cases} \tag{5}$$

$$S_t^{VPP,Bid}=\begin{cases}S_t^{VPP,E} & \text{if } S_t^{VPP,E}\ge\Phi_{ID}\\ 0 & \text{o.w.}\end{cases} \tag{6}$$

The variable $S_t^{VPP,E}$ represents the estimated VPP power supply at settlement $t$ based on the DA forecasting data (14 h ahead). The binary variable $B^{DA}$ will equal one if the DA market is more profitable than the ID market. A key issue in the planning phase is that there is no deviation from the planning data; thus, surplus power due to forecasting error does not exist. According to Equations (5) and (6), only shortage power occurs in the planning phase if $S_t^{VPP,E}$ is less than either $\Phi_{DA}$ or $\Phi_{ID}$. The shortage power can be supplied from either battery storage or the grid. Furthermore, the amount of feed-in-premium (FIP) in the planning phase is the same for both markets because the amount of VPP power supply is identical in both cases. Thus, Equation (4) is simplified in the planning phase by ignoring the effect of the FIP.

The constraints of the optimization problem are provided in Appendix B. Similar to Ref. [46], this study focuses on the operational cost (running cost) of technologies to calculate VPP profit. It is notable that the operation and maintenance costs of the storage power was insignificant compared to the wind and solar costs ($C^{VPP}$). The variable operation and maintenance cost of battery is estimated at 0.3 cents/kWh/year, while its fixed cost ranges from $6 to $20/kW/year [47]. To this end, this research skipped considering the battery costs into the calculations.

### 3.4. Stochastic trading in the ID market

In actual cases, a VPP system may unable to sell/buy its surplus/shortage power in the sequential electricity markets, such as the ID or real-time market [48]. The VPP system has a chance to adjust its bidding data in the ID market before power dispatching; Otherwise, the system operator will penalize the VPP system for any deviations from bidding data. According to Fig. 4, the probability of selling (buying) surplus (shortage) power at settlement $t$ in the ID market is represented by $\alpha_{1,\,t}$ ($\lambda_{1,\,t}$). A positive sign indicates income for the VPP system, while a negative sign indicates a cost. In the lack of adjustment in the ID market,

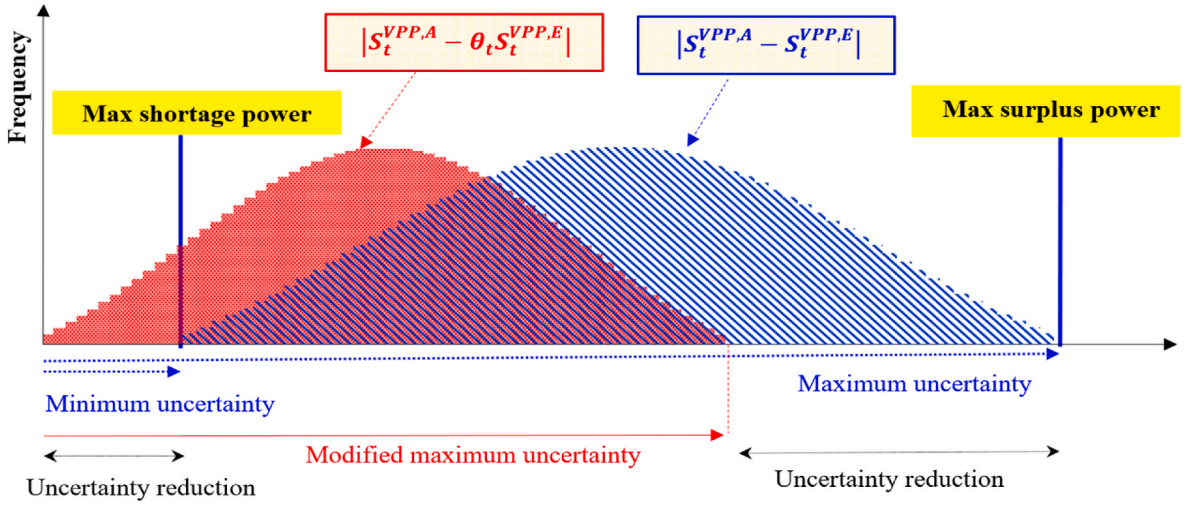


**Fig. 3.** Power prediction uncertainty versus power bidding uncertainty.

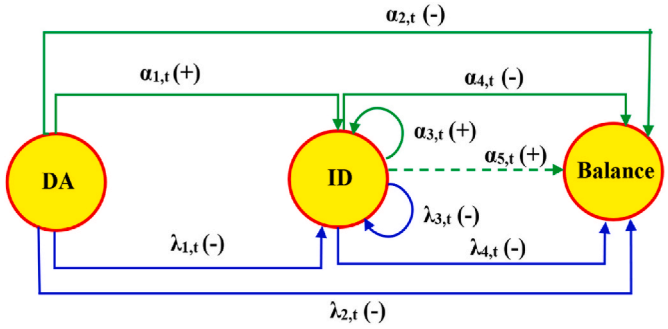


**Fig. 4.** Stochastic trading transition.

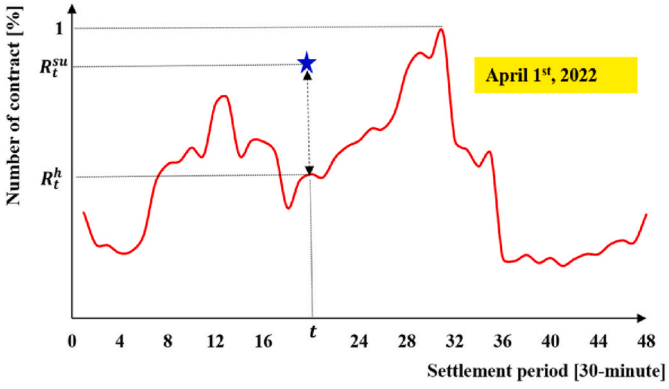


**Fig. 5.** Number of contract's percentage in each settlement.

then the VPP system will incur penalties for any remaining deviations, calculated with the following probability values (indicated as negative values in Fig. 4):

$$\begin{aligned} \alpha_{2,t} &= 1 - \alpha_{1,t} \\ \lambda_{2,t} &= 1 - \lambda_{1,t} \end{aligned} \tag{7}$$

In the case of the ID market, the VPP system may adjust its bidding with probabilities $\alpha_{3,t}$ and $\lambda_{3,t}$. The VPP system will be penalized by the ISO system for any deviations with probabilities $\alpha_{4,t}$ (=1- $\alpha_{3,t}$), and $\lambda_{4,t}$ (=1- $\lambda_{3,t}$).

According to Fig. 4, $\alpha_{5,t}$ represents the probability of selling surplus power in the balance market. As per JEPX rules, the probability of selling surplus power in the balance market is zero, i.e., $\alpha_{5,t} = 0$. However, this study assumes that small-scale VPPs can sell their surplus power in the balance market with varying probabilities, given by $\alpha_{5,t} = \{0, 0.05, 0.1, 0.2, \ldots, 0.9, 1\}$. The challenging issue is to find the trade transition probability values. One way to figure out the transition probabilities is to calculate the historical percentage of contracts in each settlement, $R_t^h$, relative to the maximum number of daily contracts in the ID market, as shown in Fig. 5. For each day, this study generates 48 random numbers, $R_t^{su}$, from the standard uniform distribution and defines the following relationships:

$$\begin{cases} \alpha_{1,t} = \alpha_{3,t} = \lambda_{1,t} = \lambda_{3,t} = 1 & \text{if } R_t^{su} \le R_t^h \\ \alpha_{2,t} = \alpha_{4,t} = \lambda_{2,t} = \lambda_{4,t} = 0 & \text{if } R_t^{su} \le R_t^h \end{cases}$$

$$\begin{cases} \alpha_{1,t} = \alpha_{3,t} = \lambda_{1,t} = \lambda_{3,t} = \dfrac{R_t^h}{R_t^{su}} & \text{if } R_t^{su} > R_t^h \\ \alpha_{4,t} = \lambda_{2,t} = \lambda_{4,t} = \left(1 - \dfrac{R_t^h}{R_t^{su}}\right) & \text{if } R_t^{su} > R_t^h \\ \alpha_{2,t} = (1 - \alpha_{5,t})\alpha_{4,t} & \text{if } R_t^{su} > R_t^h \end{cases} \tag{8}$$

It is worth mentioning that $\alpha_{5,t}$ is included in the actual profit calculation. In contrast, the planning phase assumes that the bidding data is the same as the VPP's supplied power (Equations (5) and (6)). The terms $\alpha_{1,t}$ and $\alpha_{2,t}$ are applicable when the bidding data is less than the VPP's supplied power and are not zero. This condition is not applicable in this study, but to maintain the generality of the trading transition model, they are included.

### 3.5. VPP actual profit module

This module combines the results of previous modules with the imbalance cost to calculate the actual profit of the VPP system. The following pseudocode describes the algorithm's steps used in this study to calculate the VPP actual profit for the DA market selection. It is worth mentioning that although lines 2–13 explain the battery charging and discharging processes, the actual charge and discharge occur in line 15. In other words, the forecasting data adjustments shown in Fig. 2 (for 7 h, 2 h, and 1 h) are employed to calculate the VPP's purchase (sale) of shortage (surplus) power in the ID market.

### 3.6. Data acquisition

Table 2 provides details about data type, data resolution, collected period, and their usage.

## 4. Results

This section presents the results of VPP profit with and without the UO model in which the uncertainty is measured as following:

$$Uncertainty = \sum_{i=1} |Actual_i - Prediction_i| \tag{9}$$

The results are presented in terms of production and cost, with the VPP's cost influenced by battery capacity. The following equation is used to calculate the battery capacity for three prediction models: LSTM, BiLSTM, and DSS-BiLSTM.

$$Battery\ capacity\ [Ah] = \frac{Daily\ power\ load\ [Wh] \times autonomoy\ day \times temperature\ correction\ factor}{Battery\ voltage \times Load\ subsystem\ efficiency \times DoD} \tag{10}$$

Where the daily power load is calculated as follows:

$$Average\ power\ load_t\ [Wh] = \frac{\sum_{d=1}^{579} \left| S_{t,d}^{VPP,A} - S_{t,d}^{VPP,Bid} \right|}{579} \quad t = 1, \ldots, 48 \tag{11}$$

**Daily simulation algorithm for market selection**

**Input:**

Estimation VPP supply = $\{S_t^{VPP,E14}, S_t^{VPP,E7}, S_t^{VPP,E2}, S_t^{VPP,E1}\}$; Price estimation = $\{P_t^{DA}, P_t^{ID}, P_t^{Bal}, P_t^{FIP}\}$; Transition probability = $\{R_t^{su}, R_t^{h}\}$; battery data; VPP generation cost [JPY/kWh]; Reserve capacity=5%;

2: Calculate the amount of adjustment for the second prediction as $Adj_t^{VPP,E_7} = S_t^{VPP,E_7} - S_t^{VPP,DA,Bid}$,

3: Charge/discharge maximum portion of $|Adj_t^{VPP,E_7}|$ into/out of battery if possible, and update the battery SOC,

4: Update the adjustment value after battery charging and discharging, $Adj\_Update_t^{VPP,E_7}$,

5: Calculate the ID power sale or purchase as $Sale_t^{ID,E_7} = \alpha_{3,t} Adj\_Update_t^{VPP,E_7}$ and $Buy_t^{ID,E_7} = \lambda_{3,t} Adj\_Update_t^{VPP,E_7}$,

6: Calculate the amount of adjustment for the third prediction

$$Adj_t^{VPP,E_2} = \begin{cases} S_t^{VPP,E_2} - Sale_t^{ID,E_7} + Buy_t^{ID,E_7} - S_t^{VPP,DA,Bid} & if\ S_t^{VPP,E_2} - Sale_t^{ID,E_7} + Buy_t^{ID,E_7} \geq S_t^{VPP,DA,Bid} \\ -(S_t^{VPP,DA,Bid} - (S_t^{VPP,E_2} - Sale_t^{ID,E_7} + Buy_t^{ID,E_7})) & o.w. \end{cases}$$

7: Charge/discharge maximum portion of $|Adj_t^{VPP,E_2}|$ into/out of battery if possible,

8: Update the adjustment value after battery charging and discharging, $Adj\_Update_t^{VPP,E_2}$,

9: Calculate the ID power sale or purchase as $Sale_t^{ID,E_2} = \alpha_{3,t} Adj\_Update_t^{VPP,E_2}$ and $Buy_t^{ID,E_2} = \lambda_{3,t} Adj\_Update_t^{VPP,E_2}$,

10: Calculate the amount of adjustment for the third prediction

$$Adj_t^{VPP,E_1} = \begin{cases} S_t^{VPP,E_1} - Sale_t^{ID,E_2} + Buy_t^{ID,E_2} - S_t^{VPP,DA,Bid} & if\ S_t^{VPP,E_1} - Sale_t^{ID,E_2} + Buy_t^{ID,E_2} \geq S_t^{VPP,DA,Bid} \\ -(S_t^{VPP,DA,Bid} - (S_t^{VPP,E_1} - Sale_t^{ID,E_2} + Buy_t^{ID,E_2})) & o.w. \end{cases}$$

11: Charge/discharge maximum portion of $|Adj_t^{VPP,E_1}|$ into/out of battery if possible,

12: Update the adjustment value after battery charging and discharging, $Adj\_Update_t^{VPP,E_1}$,

13: Calculate the ID power sale or purchase as $Sale_t^{ID,E_1} = \alpha_{3,t} Adj\_Update_t^{VPP,E_1}$ and $Buy_t^{ID,E_1} = \lambda_{3,t} Adj\_Update_t^{VPP,E_1}$,

14: Modify the actual VPP power supply as $S_t^{VPP,MA} = S_t^{VPP,A} + \sum_{k=1,2,7}(Buy_t^{ID,E_k} - Sale_t^{ID,E_k})$,

15: Charge or discharge difference between $S_t^{VPP,MA}$ and $S_t^{VPP,DA,Bid}$ into battery if possible,

16: Calculate total surplus or shortage power as $SuSh_t^{VPP} = S_t^{VPP,MA} - S_t^{VPP,DA,Bid} - \frac{S_t^{Bat,ch}}{\eta_{ch}^{Bat}} + S_t^{Bat,disch}\eta_{disch}^{Bat}$,

17: If $SuSh_t^{VPP} \geq 0$ then calculate the balance power sale or surplus penalty as $Sale_t^{Bal} = \alpha_{5,t} SuSh_t^{VPP}$ and $Su_t^{Penalty} = (SuSh_t^{VPP} - Sale_t^{Bal})\alpha_{4,t}$,

18: If $SuSh_t^{VPP} < 0$ then calculate the penalty of shortage power as $Sh_t^{Penalty} = -SuSh_t^{VPP}\lambda_{4,t}$,

19: Calculate total VPP cost via summing up the following cost items:

$$Power\ purchase\ from\ ID\ market = Buy_t^{ID,E_1} P_t^{ID} + Buy_t^{ID,E_2} P_t^{ID}$$
$$Penalty\ cost\ of\ balance\ market\ [surplus] = Su_t^{Penalty} P_t^{Bal}$$
$$Penalty\ cost\ of\ balance\ market\ [shortage] = Sh_t^{Penalty} P_t^{Bal}$$
$$Reserve\ capacity\ cost = S_t^{VPP,DA,Bid} P_t^{DA} \emptyset$$
$$VPP\ generation\ cost = S_t^{VPP,A} C^{VPP}$$

20: Calculate total VPP income via summing up the following cost items:

$$Bidding\ (or\ Contract)\ income = S_t^{VPP,DA,Bid} P_t^{DA} (or\ P_t^{ID})$$
$$ID\ market\ revenue\ [selling\ surplus] = Sale_t^{ID,E_1} P_t^{ID} + Sale_t^{ID,E_2} P_t^{ID}$$
$$Balance\ market\ revenue\ [selling\ surplus] = Sale_t^{Bal} P_t^{Bal}$$
$$FIP\ income = (S_t^{VPP,A} - S_t^{Bat,ch} - Su_t^{Penalty}) P_t^{FIP}$$

21: Calculate VPP profit via subtracting total VPP cost from total VPP income.

$$Daily\ power\ load\ [Wh] = Max(Average\ power\ load_{t=1}\ [Wh], \ldots, Average\ power\ load_{t=48}\ [Wh]) \quad (12)$$

Table 3 represents further details on the battery parameters and specifications used in this research.

### 4.1. Uncertainty reduction in bid data: VPP production

Fig. 6 illustrates the effect of the proposed UO model on reducing uncertainty in predictions. The reduction in uncertainty is significant for the LSTM and BiLSTM models, as their prediction accuracy is lower than that of the DSS-BiLSTM model. In contrast, the effect of the UO model on uncertainty reduction in the DSS-BiLSTM model is minimal, given that this model exhibits higher predictive accuracy compared to the LSTM and BiLSTM models[4].

[4] The symmetric mean absolute percentage error (Mean absolute error) metric values for LSTM, BiLSTM, and DSS-BiLSTM in 38 h prediction are 64 % (445,962 kW), 62 % (478,239 kW), and 50 % (261,118 kW), respectively.

**Table 2**
Data types and their sources.

| Module | Explanations |
|---|---|
| Prediction module | - VPP power generation data was collected from April 1, 2022 to March 21, 2024, at a resolution of 30 min from TEPCO website [49]. The average generation capacity of the VPP was 1.5 GW in Tokyo, Japan. Clustering was conducted on 21 months of data (April 1, 2022, to December 31, 2023). |
| Bidding module | - Uncertainty optimization was employed for 7-h ahead forecasting data<br>- Bidding data was generated for 81 days (January 1, 2024, to March 21, 2024). |
| Market selection module | - The DA and ID market prices, as well as FIP data, were obtained from the JEPX website from January 1, 2024, to March 21, 2024, at a resolution of 30 min [50]. |
| Forecasting data adjustment | - LSTM, BiLSTM, and DSS-BiLSTM models were applied to forecast VPP power generation for the last 173 days (from October 1, 2023, to March 21, 2024), with fall season data considered as the initial data for uncertainty optimization.<br>- VPP forecasting was implemented four times: 14 h before the first dispatch power, and 7 h, 2 h and 1 h ahead of each dispatch product)<br>- The number of power trading contracts was extracted from the JEPX website [50] from January 1, 2024, to March 21, 2024, at a resolution of 30 min to conduct a stochastic trading plan. |
| Dispatch module | - Based on the selected market and bidding data adjustments, actual VPP analysis was carried out for 81 days,<br>- Tokyo electric imbalance cost was gathered over January 1, 2024, to March 21, 2024, at a resolution of 30 min from the "Imbalance Cost Calculation Service" website [51]. |

**Table 3**
Battery capacity calculation data.

| | | | |
|---|---|---|---|
| Initial state of charge [%] | 100 | Day of autonomy [day] | 1 |
| Max state of charge [%] | 80 | Voltage [V] | 24 |
| Min state of charge [%] | 20 | Load subsystem efficiency [%] | 85 |
| Charging/Discharging efficiency [%] | 90 | Depth of discharge, DoD [%] | 95 |
| Temperature compensation factor | 1.19 | | |

The primary advantage of the proposed UO model lies in its capacity to adjust prediction data for models characterized by high uncertainty. VPP owners employing models with lower accuracy or greater uncertainty, such as LSTM and BiLSTM, can effectively utilize the UO model to refine their prediction data. This adjustment is achieved without necessitating the use of a more accurate predictive model, thereby offering a valuable tool for enhancing the reliability of forecasts in scenarios where high-accuracy models may be impractical due to various limitations.

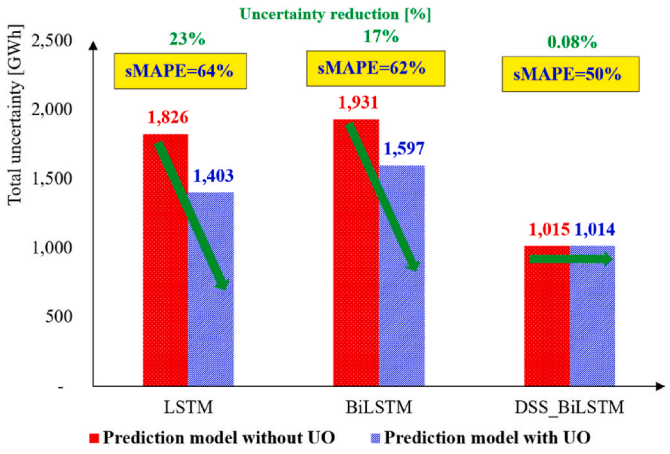


**Fig. 6.** Total uncertainty reduction over 81 days.

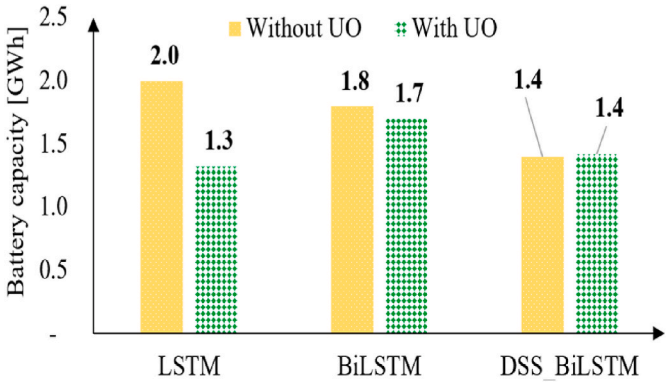


**Fig. 7.** Battery capacity with/out UO.

The UO optimization coefficients and the forecasted data are used to build the bidding data. Thus, total uncertainty reduction here implies the effectiveness of the UO model in narrowing the gap between bidding data and actual VPP power generation. The DSS-BiLSTM prediction model closely aligns with the actual VPP power generation. Thus, the effect of the UO model is almost negligible from a production insight perspective, while the total uncertainty reduction values for the LSTM and BiLSTM models are 23 % and 17 %, respectively.

Although this study considers only the operation and maintenance costs of the VPP system, Fig. 7 displays the effectiveness of the proposed UO model in reducing battery capital costs. Adjusting the initial prediction data based on the UO model's output decreases the battery capacity from 2.0 to 1.3 GWh in the LSTM model, while there is a capacity reduction of up to 0.1 GWh for the BiLSTM model. In contrast, the battery capacity remains nearly unchanged in the case of the DSS-BiLSTM model after incorporating the UO model's output into the initial DSS-BiLSTM prediction data.

Fig. 8 depicts total uncertainty reduction in terms of shortage and surplus power. It is evident that the shortage power has decreased due to the UO model in all three prediction models. Unlike the DSS-BiLSTM, the surplus power has decreased in the LSTM and BiLSTM models. If the VPP owner is able to sell the surplus power in the ID or balancing market, applying the UO model will guarantee a higher profit than the initial bidding.

### 4.2. *Uncertainty reduction in bid data: VPP cost*

The VPP profit varies with different values of $\alpha_5$, which indicates the extent to which the VPP surplus power will be sold in the balancing market.

According to Fig. 9, income derived from bidding and surplus sales in the balancing market increases the VPP income in the absence of the UO model's output. In contrast, the VPP system incurs a loss in income because of reserve capacity cost; however, its surplus sales in the ID market are higher than those without UO data. The outcome of these two issues leads to a slight growth in the total profit of the DSS-BiLSTM prediction model when UO data is present.

Fig. 10 and Fig. 11 illustrate the cost and income breakdown for the BiLSTM and LSTM prediction models. The VPP income (or cost) varies remarkably for both prediction models without UO coefficients. Although the revenue obtained from VPP bidding in the lack of UO coefficients is high, the VPP cost is also significant. In other words, the imbalance penalty mechanism in JEPX is not efficient enough to effectively mitigate uncertainty. The VPP allocates a significant portion of its income to purchase power in the ID market due to the high uncertainty of the prediction data. Meanwhile, the share of the VPP owners from the

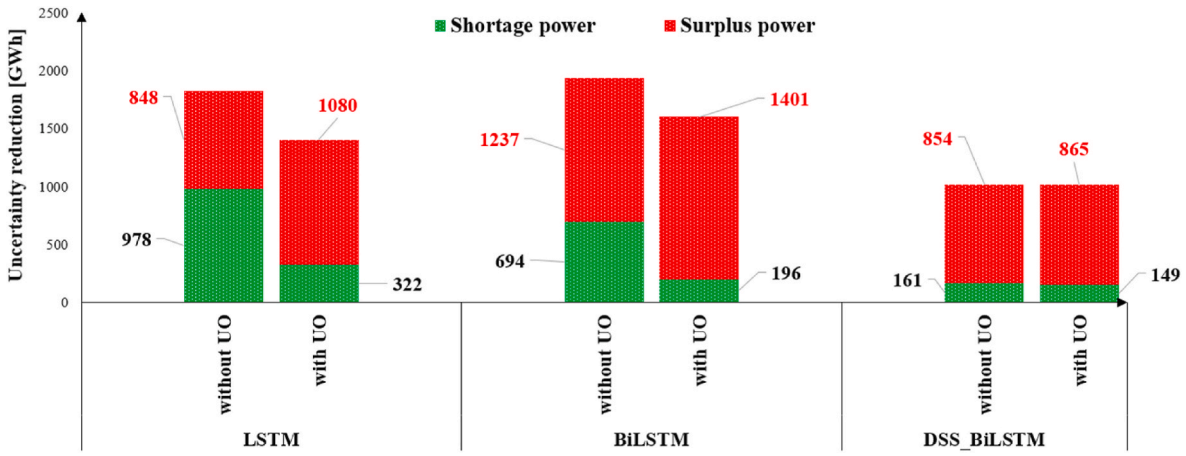


**Fig. 8.** Uncertainty reduction over 81 days in terms of surplus and shortage power.

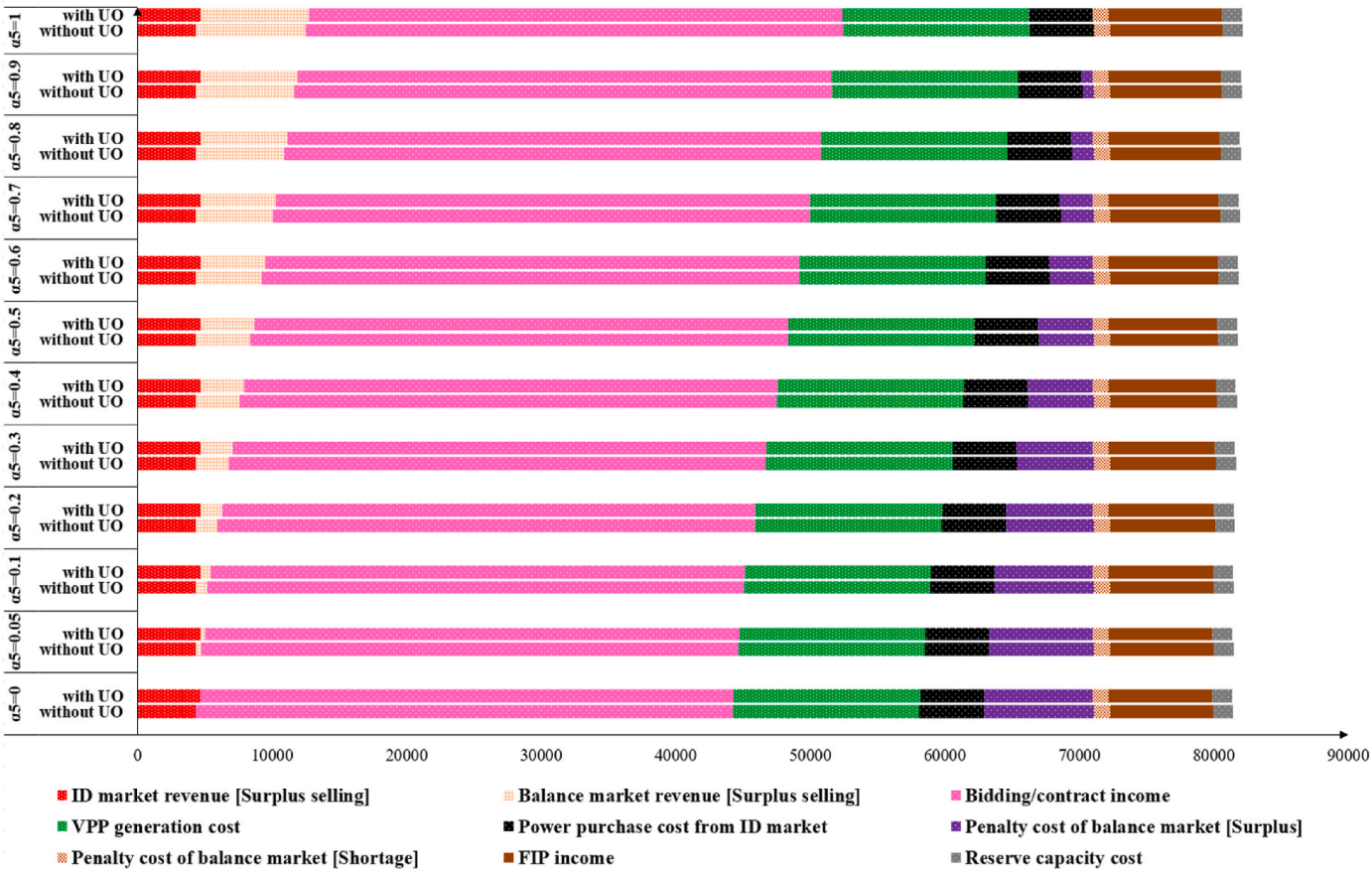


**Fig. 9.** Income and cost sources over 81 days [DSS-BiLSTM].

balancing market is insignificant because of the minimum power capacity requirement [52].

According to Figs. 10 and 11, the VPP's financial transactions in the ID market directly depend on the accuracy of the initial prediction models. Compared to the DSS-BiLSTM model, the LSTM and BiLSTM models exhibit higher sMAPE and MAE values. Thus, the VPP system using the LSTM and BiLSTM models engages with the ID market on a larger scale to balance its surplus and shortage power. In contrast, the incorporation of UO coefficients significantly decreases the scale of financial interactions in both the ID and balancing markets.

Fig. 12 displays the total actual VPP profit with and without UO coefficients. A positive value for the profit growth rate (PGR) represents that the actual profit of the VPP system under the three prediction models increases when UO coefficients are considered (Equation (13)).

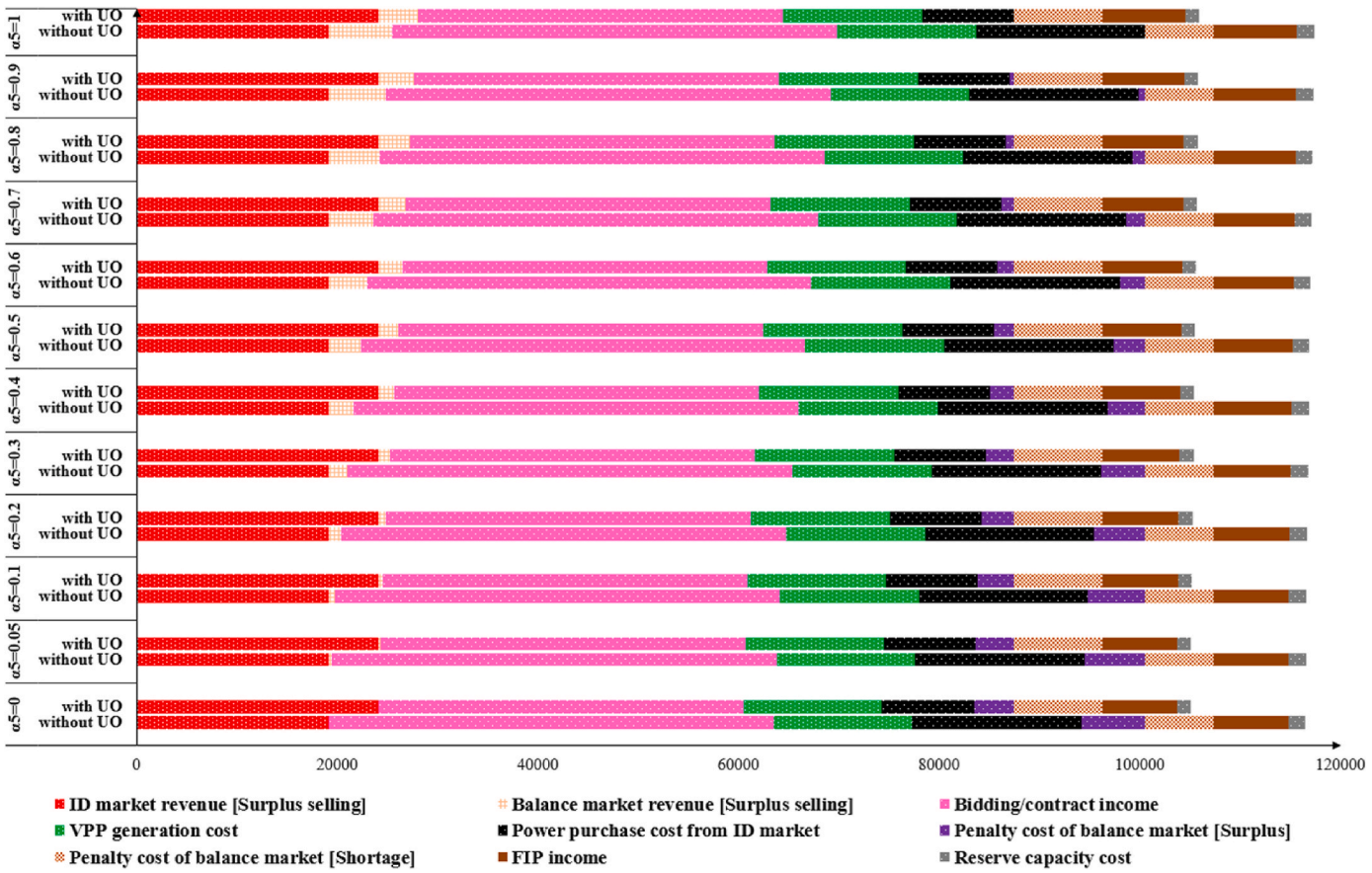


**Fig. 10.** Income and cost sources over 81 days [BiLSTM].

$$\mathrm{PGR} = \left[\left(\mathit{Actual\ Profit}_{\mathit{with\ UO}} - \mathit{Actual\ Profit}_{\mathit{without\ UO}}\right) / \mathit{Actual\ Profit}_{\mathit{without\ UO}}\right] \times 100 \tag{13}$$

However, as $\alpha_5$ approaches 100 %, the gap between actual profit with and without UO coefficients narrows. It is clear that the largest gap occurs when the probability of selling surplus power in the balancing market is at its lowest ($\alpha_5 = 0$). When $\alpha_5$ is set to this minimum value, the majority of surplus power is treated as uncertainty that is mitigated through the UO model. In contrast, as prediction accuracy increases from the LSTM model to the DSS-BiLSTM model, the effect of the UO model decreases. The slope of the black line in Fig. 12 emphasizes that the adjustment made by the UO model result in significant profit gains for the LSTM and BiLSTM models compared to the DSS_BiLSTM model. Moreover, Fig. 12 illustrates that all three models can achieve additional profit even without selling surplus power in the balancing market.

## 5. Discussion

To provide a more detailed overview of the findings of this study, the following items are discussed:

1 *Generation imbalance*: Inaccurate predictions and fluctuations in renewable energy resources increase generation imbalance. The proposed UO model can be used along with prediction models with lower accuracy and adjusts their uncertainty and reduces the generation imbalance. Reducing the generation imbalance decreases the size of energy storage significantly which saved the upstream cost of energy storage.

2 *Financial transaction in the ID and balancing markets*: the volatility of renewables always causes a gap between bidding power and actual power supply, leading to increased financial transactions in the ID and balancing markets. The proposed UO model effectively reduces this financial transaction by minimizing market uncertainty, although this uncertainty provides an arbitrage opportunity for market participants in JEPX [41].

This study primarily focused on applying the proposed UO model to VPP generation in Japan, evaluating its effectiveness in reducing uncertainty within the JEPX market. However, the UO model is broadly applicable to any VPP forecasting data, regardless of specific market conditions.

## 6. Conclusion

Even accurate prediction models are unable to remove all gaps (uncertainty) between the bidding power and actual virtual power plants (VPPs) generation. This study proposed an Uncertainty Optimization (UO) model to reduce the uncertainty associated with VPP predictions. The proposed UO model was constructed based on different weather conditions—rainy, overcast, cloudy, partly cloudy, and sunny days— across 48 market settlement periods (30 min each). The initial bidding data was generated based on three prediction models: Long Short-Term Memory (LSTM), Bidirectional LSTM (BiLSTM), and

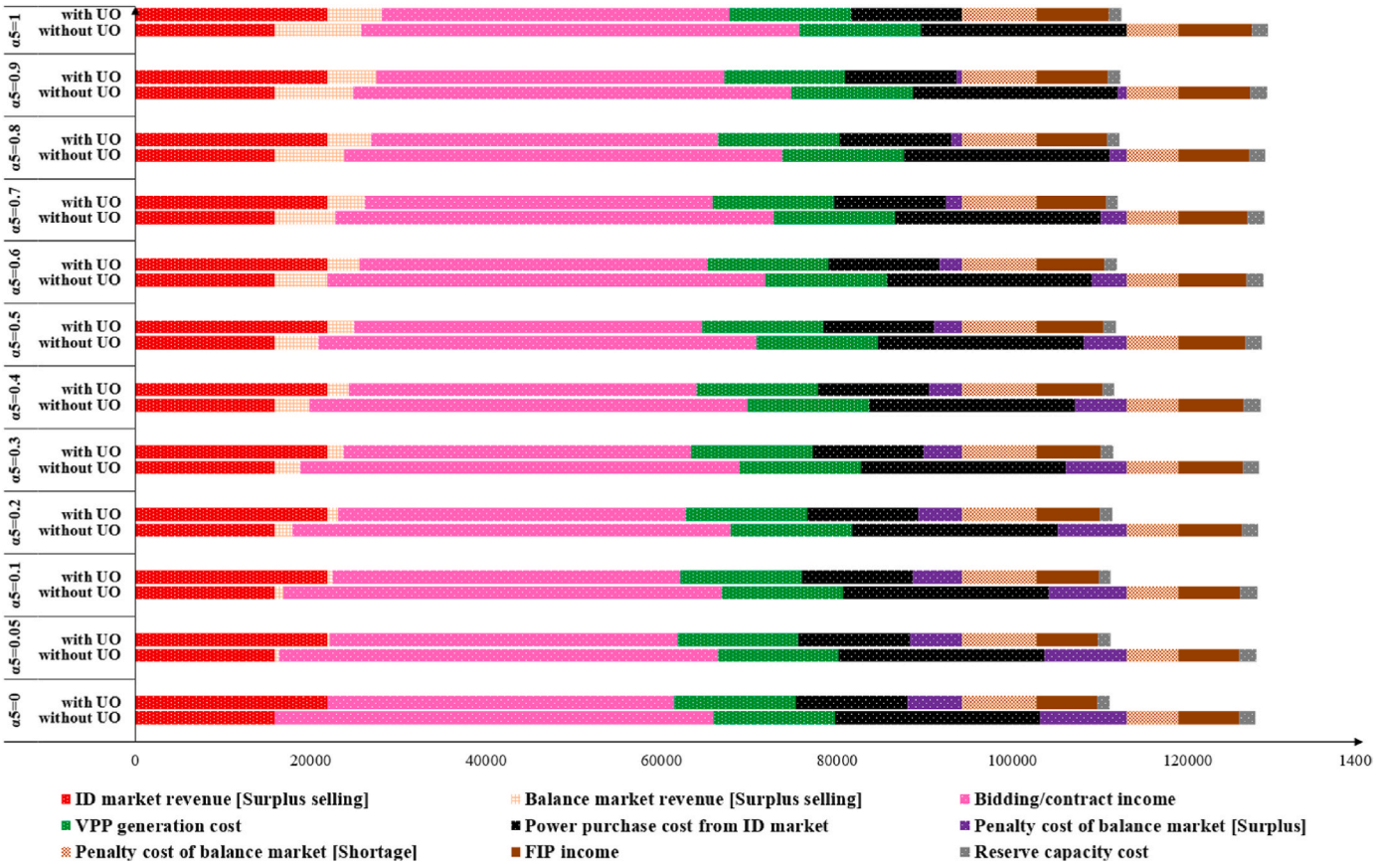


**Fig. 11.** Income and cost sources over 81 days [LSTM].

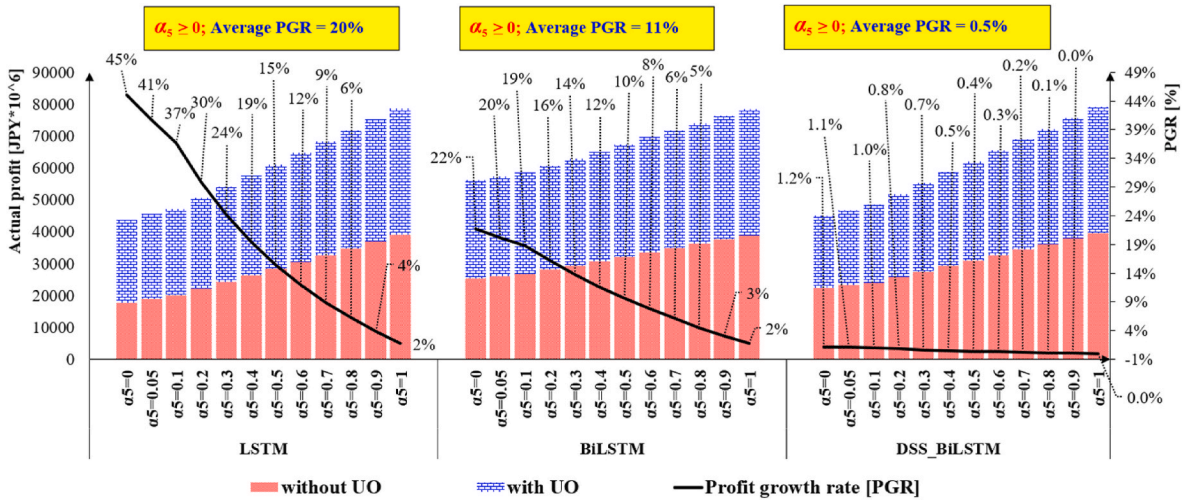


**Fig. 12.** Actual VPP profit over 81 days.

Decision Support System BiLSTM (DSS-BiLSTM). The UO model was applied to the prediction data to minimize the uncertainty of the bidding data compared to the actual VPP power supply. The effectiveness of the proposed model was evaluated in terms of additional VPP profit gained after incorporating the UO model.

The research results showed that the UO model significantly reduced uncertainty for prediction models with relatively low accuracy. Based on mean absolute error (MAE) metric, the initial prediction accuracies of the LSTM, BiLSTM, and DSS-BiLSTM models were 445,962 kW, 478,239 kW, and 261,118 kW, respectively. The total reductions in uncertainty for the LSTM, BiLSTM, and DSS-BiLSTM models were 23 %, 17 %, and 0.08 %, respectively. Notably, the uncertainty reduction was observed in the context of VPP shortage power. Specifically, the amount of shortage power decreased from 978 GWh to 322 GWh in the LSTM model, and from 694 GWh to 196 GWh in the BiLSTM model. The research findings also indicated that the implementation of the proposed UO model reduced the VPP battery capacity by up to 0.7 and 0.1 GWh in the LSTM and BiLSTM models, respectively.

The study findings indicated that actual VPP profits for the VPP increased when bidding data constructed were constructed using the UO

coefficients. This increase in the VPP profit was particularly evident in scenarios involving the sale of surplus power in the balancing market ($\alpha_5$). Although, current JEPX rules do not allow selling surplus power in the balance market, this study analyzed various scenarios for surplus power sales as $\alpha_{5,t} = \{0,0.05,0.1,0.2,\ldots,0.9,1\}$. The results showed that the average profit growth rate for the LSTM model using UO model was 20 % higher than that of the LSTM model without the UO model. The corresponding growth rates for the BiLSTM and DSS-BiLSTM models were 11 % and 0.5 %, respectively. Furthermore, the gap between actual VPP profits with and without UO coefficients decreased as the MAE value was reduced.

The main implication of the proposed model is to reduce bidding uncertainty and increase profits for VPP owners. Unlike methods that rely on hardware investment to generate profit, the proposed UO model leverages software (a mathematical model) to enhance VPP profitability. The effectiveness of the UO model in adjusting prediction data is significant, even for models with low prediction accuracy.

## CRediT authorship contribution statement

**Reza Nadimi:** Writing – review & editing, Writing – original draft, Visualization, Validation, Software, Methodology, Investigation, Formal analysis, Conceptualization. **Mika Goto:** Writing – review & editing, Supervision, Resources, Project administration, Methodology, Funding acquisition, Conceptualization.

## Declaration of competing interest

The authors declare that they have no known competing financial interests or personal relationships that could have appeared to influence the work reported in this paper.

## Acknowledgements

This work was supported by Council for Science, Technology and Innovation (CSTI), Cross-ministerial Strategic Innovation Promotion Program (SIP), the 3rd period of SIP "Smart energy management system", Grant Number JPJ012207 (Funding agency: JST).

## Appendix A. Decision Support System BiLSTM (DSS-BiLSTM) Model:

The DSS-BiLSTM model integrates the BiLSTM model with a decision support system that contains data from five weather types (WTs): rainy, overcast, cloudy, partly cloudy, and sunny days (Fig.A.2). The BiLSTM model consists of input and output matrices with ($n \times r$) and ($m \times r$), respectively as shown in Eq. (A.1) and Eq. (A.2).

$$Input\ data = \begin{bmatrix} x_{t-n+1} & x_{t-n+2} & \cdots & x_{t-n+r} \\ \vdots & \vdots & \vdots & \vdots \\ x_t & x_{t+1} & \cdots & x_{t+r-1} \end{bmatrix} \Longrightarrow \left\{X_i^{Inp}\right\} = (x_{t-n+i+1}, .., x_{t+i}) \tag{A.1}$$

$$Output\ data = \begin{bmatrix} x_{t+1} & x_{t+2} & \cdots & x_{t+r} \\ \vdots & \vdots & \vdots & \vdots \\ x_{t+m} & x_{t+m+1} & \cdots & x_{t+m+r-1} \end{bmatrix} \Longrightarrow \left\{X_i^{Out}\right\} = (x_{t+1+i}, .., x_{t+m+i}) \tag{A.2}$$

where $r$ and $m$ indicate the number of prediction times, and the number of units for ahead prediction, respectively. This study sets $m = 76$ and $n = 308$, with $i = 0, 1 \ldots, (r\text{-}1)$.

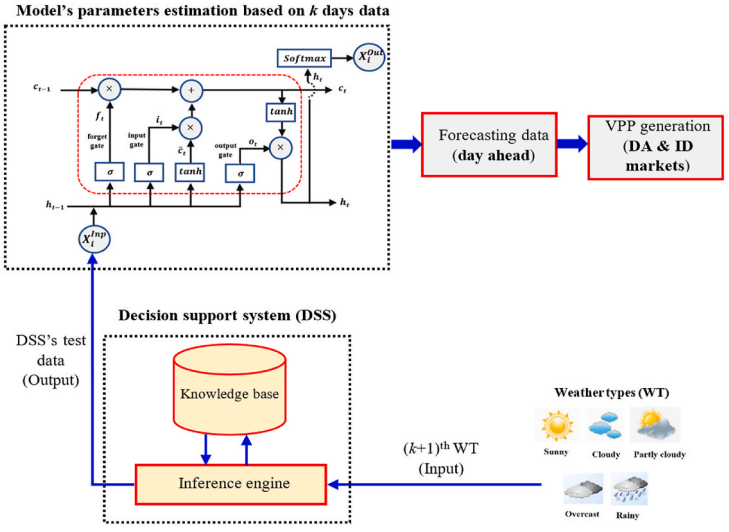


**Fig. A.2.** DSS-BiLSTM model.

**DSS system**: The DSS system is built based on the following steps:

Step1) Excute both steps outlined in the "3.1 WTs Module".

Step2) Calculate the adjusting coefficients, $\alpha_{t,WT}$, as follows:

$$\min error_t^{WT} = \sum_{l=1}^{WT} \left( x_{t,WT}^{l} - \alpha_{t,WT} \times \overline{x}_{t,WT}^{l} \right)^2 \; ; WT = \{Rainy, \ldots, Sunny\} \tag{A.3}$$

$$\overline{x}_{t,WT}^{l} = \sum_{k=l-7}^{l-1} \frac{x_{t,WT}^{k}}{7} \tag{A.4}$$

where $x_{t,WT}^{l}$ indicates the actual VPP power generation at settlement period $t$ of the $l$th day with WT type.

Step3) Build the DSS test data based on the following phases:

**Phase1)** Calculate the average WT curve for the next day through the last seven day's data stored in the knowledge base:

$$\overline{x}_{t,WT}^{k+1} = \sum_{j \in last\ 7\ WT\ day} x_t^j / 7, t = [1, 2, \ldots, 48]; k = \{7, 8, \ldots\} \tag{A.5}$$

**Phase2)** Figure out the average WT curve for the current day via the following least squares method:

$$d_t^{WT} = \sum_{t=1}^{20} \left( x_t - \overline{x}_{t,WT}^{l} \right)^2 \; ; WT = \{Rainy, \ldots, Sunny\} \tag{A.6}$$

**Phase3)** Build the DSS test data for $k$th and $(k+1)^{\text{th}}$ days with WT type:

$$DSS = \left[ \left\{ \overline{x}_{t,WT}^{k} \times \alpha_{t,WT}; t = 21, 22, \ldots, 48 \right\}, \left\{ \overline{x}_{t,WT}^{k+1} \times \alpha_{t,WT}; t = 1, 2, \ldots, 48 \right\} \right] \tag{A.7}$$

Step4) Update the last seven days of data after receiving the actual data.

Steps 1, 3, and 4 are carried out daily to update the WT types.

**BiLSTM model**: The role of the BiLSTM model is to predict VPP power generation. The DSS creates a set of test data for the BiLSTM model and retains all historical data as a training data set. The DSS test data consists of a vector with 76 elements obtained after considering the adjustment coefficients, while the training data contains a vector with 308 elements. The BiLSTM model is applied to the training data for single-step time series forecasting to calculate the model's coefficients. Then, the VPP prediction is implemented for the DSS test data via the calculated coefficients. The BiLSTM structure is similar to the LSTM model; however, the BiLSTM utilizes both forward and backward directions to calculate the weight matrix of the model. In contrast, the LSTM model uses only the forward direction. The LSTM model includes three gates (forget, input, and output gates) to remember values over time $t$, with the hidden state ($h_t$) and cell state ($c_t$). The mathematical relationships between input data, hidden state, cell state, and output data in the LSTM are as follows:

$$f_t = \sigma\left( W_h^f h_{t-1} + W_{XIn}^f X_t^{Inp} \right) \tag{A.8}$$

$$i_t = \sigma\left( W_h^i h_{t-1} + W_{XIn}^i X_t^{Inp} \right) \tag{A.9}$$

$$o_t = \sigma\left( W_h^o h_{t-1} + W_X^o X_t^{Inp} \right) \tag{A.10}$$

$$\widetilde{c}_t = tanh\left( W_h^{\tilde{c}} h_{t-1} + W_{XIn}^{\tilde{c}} X_t^{Inp} \right) \tag{A.11}$$

$$c_t = \sigma(f_t \bigodot c_{t-1} + i_t \bigodot \widetilde{c}_t) \tag{A.12}$$

$$h_t = tanh(c_t) \bigodot o_t \tag{A.13}$$

$$X_t^{Out} = softmax\left( W_h^{Xout} h_t \right) \tag{A.14}$$

where $W_{XInp}^f$ represents the weight matrix of the current input data for the forget gate. The remaining weights are interpreted similarly. Three activation functions are defined based on the following equations:

$$\sigma(inp) = {}^{1}/_{\left(1 + e^{-inp}\right)} \tag{A.15}$$

$$tanh(inp) = 1 - e^{-2inp} / \left(1 + e^{-2inp}\right) \tag{A.16}$$

$$softmax(inp_i) = e^{inp_i} \Big/ \sum_{j=1}^{n} e^{inp_j} \tag{A.17}$$

If the estimation model predicts a negative VPP power generation for a specific settlement period, the negative value will be replaced with the average value of the corresponding settlement period data from the last seven days.

*Appendix B. Constraints of the mixed integer optimization problem:*

A. *Supply-Demand balancing constraint*:

$$S_t^{VPP,Bid} - Sl_t^{Negative} + Sl_t^{Positive} = S_t^{VPP,Bid} \tag{B.1}$$

$$Sl_t^{Negative} \times Sl_t^{Positive} \leq 0 \tag{B.2}$$

$$\frac{S_t^{Bat,ch}}{\eta_{ch}^{Bat}} + Su_t^{VPP} \leq Sl_t^{Negative} \tag{B.3}$$

$$\eta_{disch}^{Bat} \times S_t^{Bat,disch} + \left(S_t^{grid,+,ID} + S_t^{grid,+,Bal}\right) \leq Sl_t^{Positive} \tag{B.4}$$

The balance between demand and supply is guaranteed via Eq. (B.1) to Eq. (B.4). Slack variables are used to adjust the amount of grid power supply and battery charging/discharging.

B. *Technological constraints of DERs*:

The study considers the total estimated and actual power supply of DERs (without access to details of each DER generation). Therefore, the technological constraints of DERs technologies are omitted.

C. *Energy storage constraints*:

$$\eta_{ch}^{Bat} \times S_t^{Bat,ch} \leq Battery\ capacity \tag{B.5}$$

$$\frac{S_t^{Bat,disch}}{\eta_{disch}^{Bat}} \leq S_{max}^{Bat,disch} \tag{B.6}$$

$$\frac{S_t^{Bat,disch}}{\eta_{disch}^{Bat}} \leq SOC_{t-1}^{Bat} \tag{B.7}$$

$$\frac{S_t^{Bat,disch}}{\eta_{disch}^{Bat}} \leq Sl_t^{Positive} \tag{B.8}$$

$$\frac{S_t^{Bat,disch}}{\eta_{disch}^{Bat}} \geq SOC_{t-1}^{Bat} - M_1 \times \left(1 - B_t^{Bat,disch}\right) \tag{B.9}$$

$$\frac{S_t^{Bat,disch}}{\eta_{disch}^{Bat}} \geq Sl_t^{Positive} - M_1 \times B_t^{Bat,disch} \tag{B.10}$$

$$\eta_{ch}^{Bat} \times S_t^{Bat,ch} \leq Battery\ capacity - SOC_{t-1}^{Bat} \tag{B.11}$$

$$\eta_{ch}^{Bat} \times S_t^{Bat,ch} \leq Sl_t^{Negative} \tag{B.12}$$

$$\eta_{ch}^{Bat} \times S_t^{Bat,ch} \geq \left(Battery\ capacity - SOC_{t-1}^{Bat}\right) - M_1 \times \left(1 - B_t^{Bat,ch}\right) \tag{B.13}$$

$$\eta_{ch}^{Bat} \times S_t^{Bat,ch} \geq Sl_t^{Negative} - M_1 \times B_t^{Bat,ch} \tag{B.14}$$

$$SOC_t^{Bat} = SOC_{t-1}^{Bat} - \frac{S_t^{Bat,disch}}{\eta_{disch}^{Bat}} + \eta_{ch}^{Bat} \times S_t^{Bat,ch} \tag{B.15}$$

$$SOC^{min} \leq SOC_t^{Bat} \leq SOC^{max} \tag{B.16}$$

$$SOC_{t=0}^{Bat} = Initial\ SOC \tag{B.17}$$

Eq. (B.5) and Eq. (B.6) set the upper bounds for the charging and discharging power of the battery in each period. Eq. (B.7) to Eq. (B.14) confine the amount of discharging and charging power into and out of the battery. Eq. (B.15) to Eq. (B.16) represent the energy balance of the battery and its boundaries. Equation (B.17) assigns the initial value for the battery's state of charge.

## References


[1] P. Denholm, T. Mai, R.W. Kenyon, B. Kroposki, M. O'Malley, Inertia and the Power Grid: A Guide without the Spin, National Renewable Energy Laboratory, 2020.

[2] R.A.v. d. Veen, R.A. Hakvoort, The electricity balancing market: exploring the design challenge, Util. Pol. 43 (2016) 186–194.

[3] Q. Wang, C. Zhang, Y. Ding, G. Xydis, J. Wang, J. Østergaard, Review of real-time electricity markets for integrating distributed energy resources and demand response, Appl. Energy 138 (2015) 695–706.

[4] C.I.S. Operator, Day-Ahead Market Enhancements: Revised Final Proposal, California ISO, California, USA, 2023.

[5] J. Katz, J. Cochran, P.K. Kumar, S. Saxena, S. Soonee, S. Narasimhan, K. Baba, Opening Markets, Designing Windows, and Closing Gates India's Power System Transition-Insights on Gate Closure, National Renewable Energy Laboratory, 2019.
[6] J. Lago, K. Poplavskaya, G. Suryanarayana, B.D. Schutter, A market framework for grid balancing support through imbalances trading, Renew. Sustain. Energy Rev. 137 (2021).
[7] R. Nadimi, M. Takahashi, K. Tokimatsu, M. Goto, The reliability and profitability of virtual power plant with short-term power market trading and non-spinning reserve diesel generator, Energies 17 (9) (2024).
[8] J. Zapata, J. Vandewalle, W. D'haeseleer, A comparative study of imbalance reduction strategies for virtual power plant operation, Appl. Therm. Eng. 71 (2) (2014) 847–857.
[9] M. Despotovic, C. Voyant, L. Garcia-Gutierrez, J. Almorox, G. Notton, Solar irradiance time series forecasting using auto-regressive and extreme learning methods: influence of transfer learning and clustering, Appl. Energy 365 (2024).
[10] N. Elamin, M. Fukushige, Modeling and forecasting hourly electricity demand by SARIMAX with interactions, Energy 165 (2018) 257–268.
[11] H. Sharadga, S. Hajimirza, R.S. Balog, Time series forecasting of solar power generation for large-scale photovoltaic plants, Renew. Energy 150 (2020) 797–807.
[12] M. Yaghoubirad, N. Azizi, M. Farajollahi, A. Ahmadi, Deep learning-based multistep ahead wind speed and power generation forecasting using direct method, Energy Convers. Manag. 281 (2023).
[13] C. Tan, Z. Tan, G. Wang, Y. Du, L. Pu, R. Zhang, Business model of virtual power plant considering uncertainty and different levels of market maturity, J. Clean. Prod. 362 (2022).
[14] S. Yu, F. Fang, Y. Liu, J. Liu, Uncertainties of virtual power plant: problems and countermeasures, Appl. Energy 239 (2019) 454–470.
[15] H. Wang, M. Xiong, H. Chen, S. Liu, Multi-step ahead wind speed prediction based on a two-step decomposition technique and prediction model parameter optimization, Energy Rep. 8 (2022) 6086–6100.
[16] H.-P. Nguyen, P. Baraldi, E. Zio, Ensemble empirical mode decomposition and long short-term memory neural network for multi-step predictions of time series signals in nuclear power plants, Appl. Energy 283 (2021).
[17] J. Hong, F. Liang, H. Yang, C. Zhang, X. Zhang, H. Zhang, W. Wang, K. Li, J. Yang, Multi- forword-step state of charge prediction for real-world electric vehicles battery systems using a novel LSTM-GRU hybrid neural network, eTransportation 20 (2024).
[18] Y. Gao, S. Miyata, Y. Akashi, Multi-step solar irradiation prediction based on weather forecast and generative deep learning model, Renew. Energy 188 (2022) 637–650.
[19] P. Oscar, P. García, L. González, G. Villa, Multi-step machine learning forecasting of power consumption and PV generation for distributed energy management applications, in: IEEE Conference Proceedings (IEEE Conf Proc), 2023. USA.
[20] X. Kong, X. Du, G. Xue, Z. Xu, Multi-step short-term solar radiation prediction based on empirical mode decomposition and gated recurrent unit optimized via an attention mechanism, Energy 282 (2023).
[21] A. Ahmed, M. Khalid, An intelligent framework for short-term multi-step wind speed forecasting based on Functional Networks, Appl. Energy 225 (2018) 902–911.
[22] S. Lu, Multi-step ahead ultra-short-term wind power forecasting based on time series analysis, in: IEEE International Conference on Computer Information and Big Data Applications (CIBDA), 2020. Guiyang, China.
[23] J. Jurasz, F. Canales, A. Kies, M. Guezgouz, A. Beluco, A review on the complementarity of renewable energy sources: concept, metrics, application and future research directions, Sol. Energy 195 (2020) 703–724.
[24] K.A. Stevens, T. Tang, E. Hittinger, Innovation in complementary energy technologies from renewable energy policies, Renew. Energy 209 (2023) 431–441.
[25] R. Nadimi, M. Goto, K. Tokimatsu, The impact of diesel operation time constraint on total cost of diesel-based hybrid renewable power system simulation model, Renew. Energy Focus 44 (2023) 40–55.
[26] A.A. Solomon, D.M. Kammen, D. Callaway, The role of large-scale energy storage design and dispatch in the power grid: a study of very high grid penetration of variable renewable resources, Appl. Energy 134 (2014) 75–89.
[27] Ø.S. Klyve, G. Klæboe, M.M. Nygård, E.S. Marstein, Limiting imbalance settlement costs from variable renewable energy sources in the Nordics: internal balancing vs. balancing market participation, Appl. Energy 350 (2023).
[28] A. Rafati, M. Joorabian, E. Mashhour, An efficient hour-ahead electrical load forecasting method based on innovative features, Energy 201 (2020).
[29] X. Xiong, X. Hu, H. Guo, A hybrid optimized grey seasonal variation index model improved by whale optimization algorithm for forecasting the residential electricity consumption, Energy 234 (2021).
[30] Seasonal variation in household electricity demand: a comparison of monitored and synthetic daily load profiles, Energy Build. 179 (2018) 292–300.
[31] A. Moradzadeh, B. Mohammadi-Ivatloo, M. Abapour, A. Anvari-Moghaddam, S. Sekhar Roy, Heating and cooling loads forecasting for residential buildings based on hybrid machine learning applications: a comprehensive review and comparative analysis, IEEE Access 10 (2022) 2196–2215.
[32] A.S. Jihad, M. Tahiri, "Forecasting the heating and cooling load of residential buildings by using a learning algorithm "gradient descent", Morocco,", Case Stud. Therm. Eng. 12 (2018) 85–93.
[33] D. McCarthy, "Independent Review on the Security of Electricity Supply," the Minister for the Environment, Climate and Communications, Irish government, 2023.
[34] J. Lago, F.D. Ridder, B.D. Schutter, Forecasting spot electricity prices: deep learning approaches and empirical comparison of traditional algorithms, Appl. Energy 221 (2018) 386–405.
[35] P. Shinde, M. Amelin, A Literature Review of Intraday Electricity Markets and Prices, IEEE, Milan, Italy, 2019.
[36] B. Uniejewski, G. Marcjasz, R. Weron, Understanding intraday electricity markets: variable selection and very short-term price forecasting using LASSO, Int. J. Forecast. 35 (2019), 1533-1457.
[37] A. Ortner, G. Totschnig, The future relevance of electricity balancing markets in Europe - a 2030 case study, Energy Strategy Rev. 24 (2019) 111–120.
[38] C. O'Connor, J. Collins, S. Prestwich, A. Visentin, Electricity price forecasting in the Irish balancing market, Energy Strategy Rev. 54 (2024).
[39] M. Petitet, M. Perrot, S. Mathieu, D. Ernst, Y. Phulpin, Impact of gate closure time on the efficiency of power systems balancing, Energy Pol. 129 (2019) 562–573.
[40] A. Facchini, A. Rubino, G. Caldarelli, G.D. Liddo, Changes to Gate Closure and its impact on wholesale electricity prices: the case of the UK, Energy Pol. 125 (2019) 110–121.
[41] T. Matsumoto, D. Bunn, Y. Yamada, Mitigation of the inefficiency in imbalance settlement designs using day-ahead prices, IEEE Trans. Power Syst. 37 (5) (2022) 3333–3345.
[42] R. Nadimi, K. Tokimatsu, Modeling of quality of life in terms of energy and electricity consumption, Appl. Energy 212 (2018) 1282–1294.
[43] E. Schubert, Stop Using the Elbow Criterion for K-Means and How to Choose the Number of Clusters Instead, 2023 [Online].
[44] G. Strbac, D.S. Kirschen, Who should pay for reserve? Electr. J. 13 (8) (2000) 32–37.
[45] Aggregation of Electricity Supply Plans for Fiscal Year 2023," Organization for Cross-Regional Coordination of Transmission Operators (OCCTO).
[46] K. Abiodun, K. Hood, J.L. Cox, A.M. Newman, A.J. Zolan, The value of concentrating solar power in ancillary services markets, Appl. Energy 334 (2023).
[47] N.D. Jackson, T. Gunda, N. Gayoso, J. Desai, A. Walker, Operations, Maintenance, and Costconsiderations for PV+Storage in the United States, Sandia National Laboratories, 2022.
[48] S.Ø. Ottesen, A. Tomasgard, S.-E. Fleten, Multi market bidding strategies for demand side flexibility aggregators in electricity markets, Energy 149 (2018) 120–134.
[49] "TEPCO power grid," TEPCO [Online]. Available, https://www.tepco.co.jp/forecast/html/area-download-j.html. (Accessed 1 November 2023).
[50] JEPX, Trading market data, Jpn. Electr. Power Exchange 28 (2003) 11 [Online]. Available: https://www.jepx.jp/electricpower/market-data/spot/. (Accessed 10 November 2023).
[51] ICS, Imbalance cost calculation service [Online]. Available: https://www.imbalanceprices-cs.jp/. (Accessed 25 December 2023).
[52] Y. Sakuma, Japanese Energy Market: Optimum Use of Distributed Energy Resources for Demand Side Response, Ministry of Economy, Trade and Industry, 2021.